Dominance of many-body effects over the one-electron mechanism for band structure doping dependence in $Nd_{2-x}Ce_xCuO_4$: the LDA+GTB approach

2007 J. Phys.: Condens. Matter 19 486203

(http://iopscience.iop.org/0953-8984/19/48/486203)

IOP PUBLISHING JOURNAL OF PHYSICS: CONDENSED MATTER

J. Phys.: Condens. Matter **19** (2007) 486203 (13pp) doi:10.1088/0953-8984/19/48/486203

Dominance of many-body effects over the one-electron mechanism for band structure doping dependence in $Nd_{2-x}Ce_xCuO_4$: the LDA + GTB approach

M M Korshunov[1,2], V A Gavrichkov[1], S G Ovchinnikov[1], I A Nekrasov[3], E E Kokorina[3] and Z V Pchelkina[4]

[1] L V Kirensky Institute of Physics, Siberian Branch of Russian Academy of Sciences, 660036 Krasnoyarsk, Russia
[2] Max-Planck-Institut für Physik komplexer Systeme, D-01187 Dresden, Germany
[3] Institute of Electrophysics, Russian Academy of Sciences-Ural Division, 620016 Yekaterinburg, Amundsena 106, Russia
[4] Institute of Metal Physics, Russian Academy of Sciences-Ural Division, 620041 Yekaterinburg, GSP-170, Russia

E-mail: maxim@mpipks-dresden.mpg.de (M M Korshunov)

Received 4 May 2007, in final form 10 September 2007
Published 6 November 2007
Online at stacks.iop.org/JPhysCM/19/486203

Abstract

In the present work we report band structure calculations for the high-temperature superconductor $Nd_{2-x}Ce_xCuO_4$ in the regime of strong electronic correlations within an LDA + GTB method, which combines the local density approximation (LDA) and the generalized tight-binding method (GTB). The two mechanisms of band structure doping dependence were taken into account. Namely, the one-electron mechanism provided by the doping dependence of the crystal structure, and the many-body mechanism provided by the strong renormalization of the fermionic quasiparticles due to the large on-site Coulomb repulsion. We have shown that, in the antiferromagnetic and in the strongly correlated paramagnetic phases of the underdoped cuprates, the main contribution to the doping evolution of the band structure and Fermi surface comes from the many-body mechanism.

(Some figures in this article are in colour only in the electronic version)

1. Introduction

It is well known that the hole doping of $La_{2-x}Sr_xCuO_4$ and the electron doping of $Nd_{2-x}Ce_xCuO_4$ shift them into the superconducting state. With the increase of doping concentration x the band structure undergoes dramatic changes from an antiferromagnetic (AFM) insulator to a normal paramagnetic metal. It is well established that the strong electronic correlations play one of the main roles in the formation of the electronic structure of high-T_c

cuprates. They are important especially for small x values and should be taken into account in the calculations explicitly.

In the present paper to study the band structure of $Nd_{2-x}Ce_xCuO_4$, we apply the LDA + GTB computational scheme [8]. This scheme combines *ab initio* calculations within the local density approximation (LDA) and the many-body generalized tight-binding (GTB) approach [9]. Earlier, within the GTB method, a specific many-body mechanism of band structure evolution for the doped Mott–Hubbard insulator was found. This mechanism is caused by the changes of occupation factors of many-body electronic terms by the quasiparticle excitations [9]. For $Nd_{2-x}Ce_xCuO_4$ such terms are the $d^{10}p^6$ term (zero holes per unit cell) and the hybridized $d^9p^6 + d^{10}p^5$ term (one hole per unit cell). Here we highlight also the so-called 'one-electron' mechanism of band structure doping dependence. It originates from the changes of a crystal structure (lattice parameters, atomic positions) upon doping. As a result, matrix elements of d–d, p–d, and p–p hybridization (hoppings, and all the rest depending on the interatomic distance) vary with doping. In the absence of strong electronic correlations, this mechanism will be responsible for the evolution of band structure with doping in the framework of the standard band theory. That is why we call it the one-electron mechanism.

Previously, the band structure of $Nd_{2-x}Ce_xCuO_4$ was considered within the LDA calculations [1–3] and the tight-binding approach [4]. Note, our approach is significantly different from these two and their simple combination. From the LDA band structure we extract the doping-dependent tight-binding parameters using a projection procedure, not fitting. Then, we use a *many-body* tight-binding computational scheme called the GTB approach. One should not mix up the one-electron tight-binding approach and the many-body GTB method. Details of the latter will be given in the next section.

To our knowledge there are no band structure calculations for the high-T_c cuprates that take both one-electron and many-body mechanisms into account. In the present paper we report the results of such calculations for $Nd_{2-x}Ce_xCuO_4$ and compare them with the simplified calculations which do not contain the one-electron mechanism. It was found that in the antiferromagnetic phase for small doping concentrations, $x \leqslant 0.1$, the one-electron mechanism results in a slight shift of the bottom of the conduction band and, simultaneously, in a small shift of the top of the valence band, thus retaining the value of the charge-transfer gap. For higher doping concentrations, the paramagnetic spin-liquid phase was considered in an approximation taking the static spin–spin correlation functions into account. In this phase, the one-electron mechanism provides small changes in the bandwidth. However, the Fermi surface and critical concentrations at which the Fermi surface topology changes, remain the same as in the case when the one-electron mechanism is disregarded.

2. Brief description of a hybrid LDA + GTB computational scheme

Ab initio electronic structure calculations within the density functional theory have their development within the LDA approximation. This approximation does not take strong electronic correlations into account properly. That is why the true band structure of Mott insulators cannot be described within the LDA. We employ the LDA to calculate the non-interacting part of the multiband p–d model Hamiltonian. Then, the strong electronic correlations enter into the framework of the GTB approach [8].

LDA + GTB method consists of the following steps:

(i) *Ab initio* LDA band structure calculation, finding of Bloch functions;

(ii) construction of the Wannier functions for the physically relevant states;

Table 1. Crystal structure parameters (Å) for $Nd_{2-x}Ce_xCuO_4$ for different Ce concentrations (see [11, 12]).

Lattice constant	$x = 0.00$	0.05	0.10	0.15	0.20	0.30
a	3.943 62	3.940 56	3.940 71	3.942 24	3.942 95	3.942 88
c	12.1584	12.1130	12.0945	12.0603	12.030	12.0288
z (Nd)	0.35112	0.3519	0.3523	0.3527	0.3531	0.3531

(iii) construction of the multiband p–d model Hamiltonian with the parameters obtained from the previous two steps;
(iv) splitting of the multiband p–d model Hamiltonian into a sum of inter- and intra-cell components and exact diagonalization of the intra-cell part in order to construct the many-body molecular orbitals for the unit cell;
(v) construction of the intra-cell Hubbard X-operators on the basis of these molecular orbitals and rewriting the full Hamiltonian for the crystal in the X-representation;
(vi) calculation of a quasiparticle band structure for Hubbard fermions in the framework of the perturbation theory with small inter-cell hopping and interactions.

Note, the first version of the GTB method [9, 10] contained a large number of unknown model parameters, which were extracted by comparison with experimental data. In the generalized LDA + GTB method, all parameters of the theory are calculated explicitly. For a given doping concentration x we calculate the *ab initio* band structure. The one-electron mechanism of band structure doping dependence is determined by the dependence of the matrix elements of the interatomic hopping and one-electron energies on doping, which is due to the change of the lattice parameters with x. The many-body mechanism arises from the doping dependence of the occupation factors. Thus, the one-electron mechanism takes place for the ordinary tight-binding method while the many-body mechanism appears within the GTB method as the effect of the strong electronic correlations.

3. Electronic structure and model parameters of $Nd_{2-x}Ce_xCuO_4$: LDA results

Nd_2CuO_4 crystallizes in tetragonal structure with the symmetry space group $I4/mmm$ [11], also called the T'-structure. Lattice parameters are $a = b = 3.943\,62$ Å, and $c = 12.1584$ Å [11]. Cu ions in positions 2a, $(0, 0, 0)$, are surrounded by four ions of oxygen O1, which occupy positions 4c, $(0, 0.5, 0)$. Ions of Nd in positions 4e, $(0, 0, 0.35112)$, have eight nearest neighbors of oxygen O2 in positions 4d, $(0, 0.5, 0.25)$. In comparison with the high-temperature tetragonal structure of La_2CuO_4, in the T'-structure of Nd_2CuO_4 the apical oxygen ions around Cu ions are absent. With Ce doping the symmetry group of $Nd_{2-x}Ce_xCuO_4$ remains the same whereas the lattice parameters and z-coordinate of Nd positions are changing (see table 1) [11, 12].

Electronic structure of $Nd_{2-x}Ce_xCuO_4$ at $0 \leqslant x \leqslant 0.3$ was calculated using the local density approximation. To this end, the linearized muffin-tin orbitals (LMTO) method in the tight-binding approach within the atomic spheres approximation (TB–LMTO–ASA) was applied [13, 14]. The 4f states of Nd were considered as semi-core states, because they are well localized and are situated far below the Cu-d states [15]. The LDA band structure of $Nd_{2-x}Ce_xCuO_4$ along the high symmetry directions of the Brillouin zone is shown in figure 1 with gray dashed curves. Bands formed by the hybridized 3d copper and 2p oxygen states have a width of approximately 9 eV. As a result of hybridization between the $d_{x^2-y^2}$ copper orbital and appropriate $p_{x,y}$ orbitals of plain oxygen (O1), the bonding bands are located at

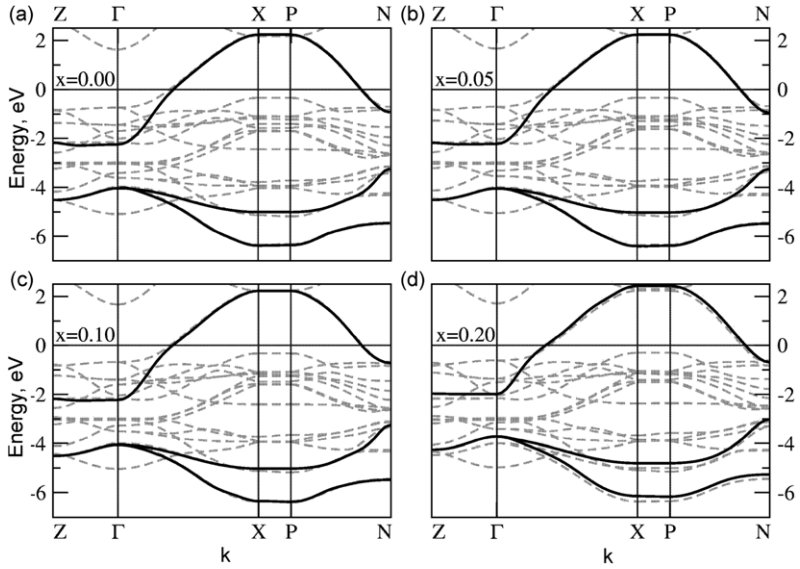

Figure 1. Comparison of the electronic dispersion obtained within the LDA calculations (gray dashed curves) and the electronic dispersion of the effective non-interacting three-band Hamiltonian for the NMTO orbitals basis set (black solid curves) for different Ce concentrations x.

energies $-5\cdots-6$ eV, while the antibonding bands cross the Fermi level. These hybrid orbitals determine the non-interacting Hamiltonian of the so-called three-band p–d model [16, 17].

To calculate hopping integrals for the three-band p–d model, the NMTO (muffin-tin orbitals of Nth order) [18] method was used. For the three physically relevant hybrid bands (Cu-$d_{x^2-y^2}$ and O1-$p_{x,y}$) the NMTO orbitals were constructed. Corresponding band dispersions are shown in figure 1 by solid black curves. Observe, that NMTO orbitals almost perfectly reproduce the LDA calculated bonding and antibonding bands formed by hybrid $d_{x^2-y^2}$ copper and $p_{x,y}$ oxygen orbitals. Thus, within this NMTO basis we have obtained an effective few-orbital Hamiltonian, the three-band p–d model, which we were looking for.

Note, we do not take into account the Cu-4s orbitals explicitly. Their importance for the bilayer cuprates was shown in [5–7]. For bilayer structures, the 4s states connect two neighboring CuO_2-layers. It is not the case for $Nd_{2-x}Ce_xCuO_4$, the system where there is only one CuO_2-layer per unit cell. Moreover, due to the absence of apical oxygens this layer becomes even more two-dimensional. There is also a contribution from the Cu-4s states to the in-plane hopping integrals [4]. However, in paper [5] it was shown that one can do the so-called Loewdin transformation and end up with the three-band p–d model with the renormalized parameters. Since our tight-binding parameters are not fitted but calculated within the NMTO method from the full-band LDA results, such a renormalization is automatically performed. Thus, we partially take into account the Cu-4s states implicitly.

Having applied the Fourier transform to this effective Hamiltonian in momentum space we obtain the real space hopping integrals depending on the distances between atoms (see table 2). From figure 1 and table 2 one can conclude that hopping integrals change with doping slightly. It allows us to assume that the one-electron contribution to the evolution of $Nd_{2-x}Ce_xCuO_4$ electronic structure with increase of Ce concentration is not substantial.

For the three-band p–d model we also need the values of Coulomb repulsion U and Hund's exchange parameter J_H for Cu ions. In the paper [19] they were calculated for copper in the

Table 2. Hopping integrals and one-electron energies (eV) as a function of Ce concentration for $Nd_{2-x}Ce_xCuO_4$ obtained by the NMTO method. Here x^2, p_x, p_y denote the Cu-$d_{x^2-y^2}$ and O1-$p_{x,y}$ orbitals respectively.

		$x = 0.00$	0.05	0.10	0.15	0.20	0.30
Energy							
$E(x^2)$		−2.2855	−2.2847	−2.1760	−2.4215	−2.3507	−2.3234
$E(p_x)$		−3.2935	−3.3064	−3.2829	−3.2607	−3.2800	−3.2957
Hopping	Direction						
$t(x^2, p_x)$	(0.5, 0)	1.1216	1.1454	1.1665	1.1614	1.1726	1.1719
$t'(x^2, p_x)$	(0.5, 1)	−0.0504	−0.0359	−0.0211	−0.0202	−0.0166	−0.0201
$t''(x^2, p_x)$	(1.5, 0)	0.0834	0.0921	0.1173	0.1130	0.1203	0.1126
$t'''(x^2, p_x)$	(1.5, 1)	−0.0149	−0.0083	0.0015	0.0090	0.0153	0.0099
$t(p_x, p_y)$	(0.5, 0.5)	0.8320	0.8389	0.8381	0.8365	0.8386	0.8304
$t'(p_x, p_y)$	(1.5, 0.5)	0.0266	0.0331	0.0452	0.0450	0.0469	0.0388

La_2CuO_4 compound by a super-cell method [20] and equal to: $U = 10$ eV, $J_H = 1$ eV. We presume these values to be doping independent and use them in the present paper for the $Nd_{2-x}Ce_xCuO_4$ compound.

4. LDA + GTB results in the AFM phase

For the wide range of doping concentrations $Nd_{2-x}Ce_xCuO_4$ remains in the AFM phase. Therefore, we will consider the evolution of the band structure with doping in the AFM phase first. Within the GTB method for this phase we use the Hubbard-I approximation [21], though the diagram technique for the X-operators [22–24] allows one to go beyond this approximation.

To write down the model Hamiltonian we use the Hubbard X-operators [25]: $X_f^{\alpha} \leftrightarrow X_f^{n,n'} \equiv |n\rangle\langle n'|$. Here index $\alpha \leftrightarrow (n, n')$ enumerates quasiparticles with energy $\omega_{\alpha} = \varepsilon_n(N+1) - \varepsilon_{n'}(N)$, where ε_n is the nth energy level of the N-electron system. The commutation relations between X-operators are quite complicated, i.e. two operators commute on another operator, not a c-number. Nevertheless, depending on the difference of the number of fermions in states n and n' it is possible to define quasi-Fermi and quasi-Bose type operators in terms of obeyed statistics. There is a simple correspondence between X-operators and the single-electron annihilation operators: $a_{f\lambda\sigma} = \sum_{\alpha} \gamma_{\lambda\sigma}(\alpha) X_f^{\alpha}$, where the coefficients $\gamma_{\lambda\sigma}(\alpha)$ determine the partial weight of the quasiparticle α with spin σ and orbital index λ. These coefficients are calculated straightforwardly within the GTB scheme.

In the Hubbard-I approximation, the dispersion equation for the band structure of the Hubbard fermions in the AFM phase with the sublattices A and B is the following [10]:

$$\left\| \left(E - \Omega_{\alpha}^{B}\right) \delta_{\alpha\beta} / F_{\alpha}^{B} - 2 \sum_{\lambda\lambda'} \gamma_{\lambda\sigma}^{*}(\alpha) T_{\lambda\lambda'}^{AB}(\vec{k}) \gamma_{\lambda'\sigma}(\beta) \right\| = 0, \tag{1}$$

where Ω_{α}^{B} is the intra-cell local energy of the Hubbard fermion and $T_{\lambda\lambda'}^{AB}(\vec{k})$ is the Fourier transform of the matrix element of the intra-cell hopping between the one-electron orbitals λ and λ'. The occupation factor, F_{α}^{B}, is equal to the sum of the occupancies of initial and final many-body states, the transition between which is described by the operator X_f^{α}.

Since the structure of dispersion equation (1) is similar to the equation in the one-electron tight-binding approach, our method was called the generalized tight-binding (GTB) method.

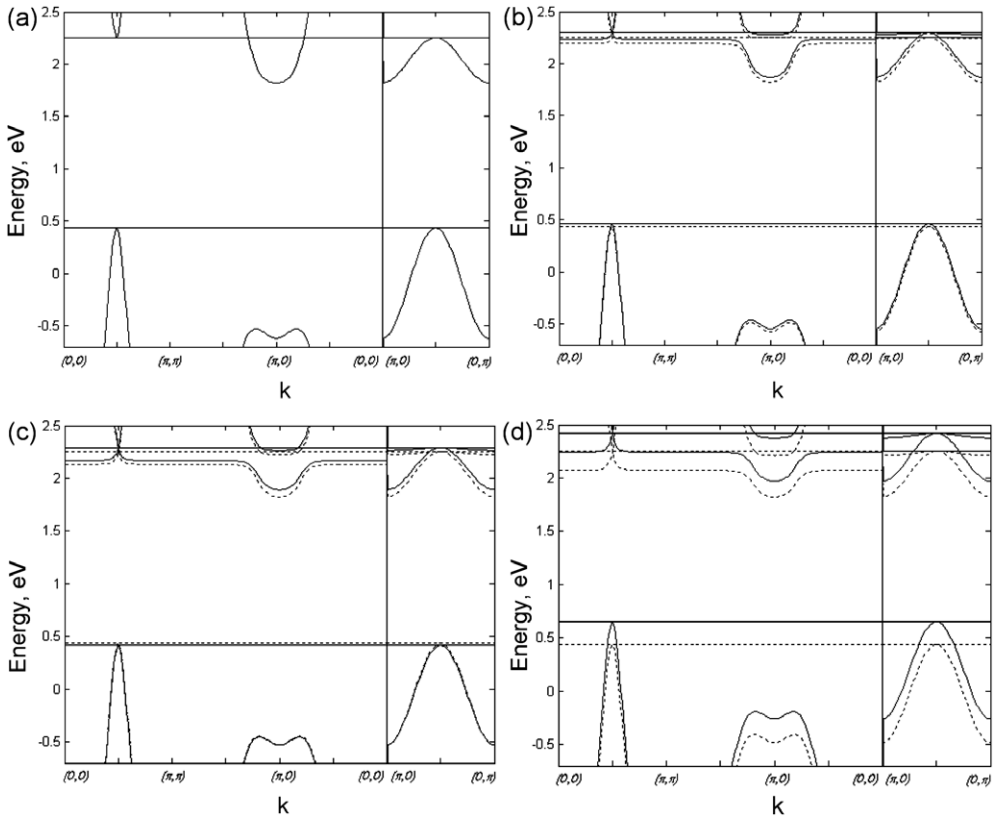

Figure 2. The quasiparticle energy momentum dependence calculated within the LDA + GTB method for $x = 0$ (a), $x = 0.05$ (b), $x = 0.1$ (c), and $x = 0.15$ (d). The dotted curve corresponds to the calculation without the one-electron mechanism of concentration dependence. The solid curve represents the results of calculations in which both many-body and one-electron mechanisms were considered.

At the same time, there are important distinctions of equation (1) from its one-electron analog. Namely, the local energies $\Omega_\alpha^{\mathrm{B}}$ are calculated with explicit consideration of strong electronic correlations inside the cell. Thus, the corresponding occupation factor can have non-integer values and it depends on temperature and doping concentration. As a result, the doping dependence of the electronic structure is not described by the rigid band model, so the effect of doping is not only due to the shift of a chemical potential for a given band structure. There are bands with the spectral weight proportional to x for small doping concentrations. These bands appear inside the dielectric gap near the bottom of the conduction band for n-type cuprates and near the top of the valence band in hole-doped cuprates. These states are called 'in-gap states' [9, 10, 26]. Note, they are not an impurity state of a doped semiconductor formed in the presence of a defect since no defects are present in our model. An example of the in-gap states near the bottom of the conduction band in $Nd_{2-x}Ce_xCuO_4$ will be discussed later in this section.

The results of the LDA + GTB calculations of the dispersion using equation (1) in the Néel state are shown in figure 2. In each figure for a given doping concentration the results of two calculations are shown: (i) with the model parameters calculated for $x = 0$ (i.e. in the absence of the one-electron mechanism but with the many-body mechanism taken into account), and (ii)

for the model parameters which depend on the concentration (see table 2), also taking the many-body mechanism into account. In the former case, the doping dependence is determined only by the doping dependence of the occupation factors, F_α^{B}, while in the latter case the dependence of matrix elements $T_{\lambda\lambda'}^{\mathrm{AB}}(\vec{k})$ on doping was also taken into account.

The results of the electronic structure calculations for an undoped compound, figure 2(a), reproduce the main effects of the strong electronic correlations in this material. On the bottom of the conduction band and on the top of the valence band there are in-gap states with spectral weight proportional to the doping level [9, 10, 26]. Upon increase of doping concentration, the in-gap state at the bottom of the conduction band becomes dispersive with non-zero spectral weight (see figures 2(b)–(d)).

For each concentration one can notice that 'switching-off' the one-electron mechanism leads to a shift of the top of the valence band and the bottom of the conduction band. This shift is almost uniform and its value is very small. Also, this does not prevent the appearance of the in-gap states. Thus, one can conclude that such fine tuning of the Hamiltonian parameters just gives a shift of the electronic structure as a whole in the vicinity of the dielectric gap. This is most probably not very important for the physics of the high-T_{c} materials.

5. Paramagnetic phase

To treat a spin-liquid phase, the multiband p–d model Hamiltonian was mapped onto an effective low-energy model [8]. Parameters of this effective model are obtained directly from the *ab initio* parameters of the multiband model. The low-energy model for n-type cuprates is the t–t'–t''–J^* model (t–t'–t''–J model with the three-site correlated hoppings) with the following Hamiltonian in the hole representation:

$$H = \sum_{f,\sigma} (\varepsilon_0 - \mu)\, X_f^{\sigma,\sigma} + \sum_{f\neq g,\sigma} t_{fg} X_f^{\sigma,0} X_g^{0,\sigma} + \sum_{f\neq g} J_{fg} \left(\vec{S}_f \vec{S}_g - \tfrac{1}{4} n_f n_g \right) + H_3. \tag{2}$$

Here μ is the chemical potential, $\vec{S}_f$ is the spin operator, $S_f^+ = X_f^{\sigma,\bar{\sigma}}$, $S_f^- = X_f^{\bar{\sigma},\sigma}$, $S_f^z = \frac{1}{2}(X_f^{\sigma,\sigma} - X_f^{\bar{\sigma},\bar{\sigma}})$, $n_f = \sum_\sigma X_f^{\sigma,\sigma}$ is the number of particles operator, $J_{fg} = 2\tilde{t}_{fg}^2/E_{\mathrm{ct}}$ is the exchange parameter, $E_{\mathrm{ct}} = 2$ eV is the charge-transfer gap. In the notations of [8], the hopping matrix elements t_{fg} correspond to $-t_{fg}^{00}$, and $\tilde{t}_{fg} = -t_{fg}^{0S}$. The Hamiltonian H_3 contains the three-site interaction terms:

$$H_3 = \sum_{f\neq g\neq m,\sigma} \frac{\tilde{t}_{fm}\tilde{t}_{mg}}{E_{\mathrm{ct}}} \left(X_f^{\sigma 0} X_m^{\bar{\sigma}\sigma} X_g^{0\bar{\sigma}} - X_f^{\sigma 0} X_m^{\bar{\sigma}\bar{\sigma}} X_g^{0\sigma} \right). \tag{3}$$

In the considered case there is only one Fermi-type quasiparticle, $\alpha = (0,\sigma)$, with $\gamma_{\lambda\sigma}(\alpha) = 1$, and the Hamiltonian in the general form in the momentum representation is given by:

$$H = \sum_{\vec{k},\sigma} (\varepsilon_0 - \mu)\, X_{\vec{k}}^{\sigma,\sigma} + \sum_{\vec{k}} \sum_{\alpha,\beta} t_{\vec{k}}^{\alpha\beta} X_{\vec{k}}^{\alpha\,\dagger} X_{\vec{k}}^{\beta} + \sum_{\vec{p},\vec{q}} \sum_{\alpha,\beta,\sigma,\sigma'} V_{\vec{p}\vec{q}}^{\alpha\beta,\sigma\sigma'} X_{\vec{p}}^{\alpha\,\dagger} X_{\vec{p}-\vec{q}}^{\sigma,\sigma'} X_{\vec{q}}^{\beta}. \tag{4}$$

The Fourier transform of the two-time retarded Green function in the energy representation, $G_\lambda(\vec{k}, E) = \langle\langle a_{\vec{k}\lambda\sigma} | a_{\vec{k}\lambda\sigma}^\dagger \rangle\rangle_E$, can be rewritten in terms of the matrix Green function, $[\hat{D}(\vec{k}, E)]_{\alpha\beta} = \langle\langle X_{\vec{k}}^{\alpha} | X_{\vec{k}}^{\beta\,\dagger} \rangle\rangle_E$:

$$G_\lambda(\vec{k}, E) = \sum_{\alpha,\beta} \gamma_{\lambda\sigma}(\alpha) \gamma_{\lambda\sigma}^*(\beta) D^{\alpha\beta}(\vec{k}, E). \tag{5}$$

The generalized Dyson equation for the Hubbard X-operators [24] in the paramagnetic phase ($\langle X_0^{\sigma,\sigma}\rangle = \langle X_0^{\bar\sigma,\bar\sigma}\rangle$) reads:

$$\hat D(\vec k, E) = \left[\hat G_0^{-1}(E) - \hat P(\vec k, E)\hat t_{\vec k} - \hat P(\vec k, E)\hat V_{\vec k\vec k}^{\sigma,\sigma}\langle X_0^{\sigma,\sigma}\rangle + \hat\Sigma(\vec k, E)\right]^{-1}\hat P(\vec k, E). \tag{6}$$

Here, $\hat G_0^{-1}(E)$ is the exact local Green function, $G_0^{\alpha\beta}(E) = \delta_{\alpha\beta}/[E - (\varepsilon_n - \varepsilon_{n'})]$, $\hat\Sigma(\vec k, E)$ and $\hat P(\vec k, E)$ are the self-energy and the strength operators, respectively. The presence of the strength operator is due to the redistribution of the spectral weight between the Hubbard subbands, that is an intrinsic feature of the strongly correlated electron systems. It also should be stressed that $\hat\Sigma(\vec k, E)$ in equation (6) is the self-energy in the X-operator representation and therefore it is different from the self-energy entering the Dyson equation for the weak coupling perturbation theory for $G_\lambda(\vec k, E)$.

To calculate the strength operator $\hat P(\vec k, E)$ we use the zero-loop approximation given by the replacement: $P^{\alpha\beta}(\vec k, E) \to P^{\alpha\beta} = \delta_{\alpha\beta}F_\alpha$, where $F_{\alpha(n,n')} = \langle X_f^{n,n}\rangle + \langle X_f^{n',n'}\rangle$ is the occupation factor. Taking into account that in the considered paramagnetic phase $\langle X_f^{\sigma,\sigma}\rangle = \frac{1-x}{2}$, $\langle X_f^{0,0}\rangle = x$, after all substitutions and treating all $\vec k$-independent terms as the chemical potential renormalization, the generalized Dyson equation for the Hamiltonian (2) becomes:

$$D(\vec k, E) = \frac{(1+x)/2}{E - (\varepsilon_0 - \mu) - \frac{1+x}{2}t_{\vec k} - \frac{1+x}{2}\frac{\tilde t_{\vec k}^2}{E_{\rm ct}}\frac{1-x}{2} + \Sigma(\vec k, E)}. \tag{7}$$

To go beyond the Hubbard-I approximation we have to calculate $\Sigma(\vec k, E)$. This was done in [27] using an equations of motion method for the X-operators [28]. The calculations resulted in the following expression:

$$\Sigma(\vec k) = \frac{2}{1+x}\frac{1}{N}\sum_{\vec q}\left\{\left[t_{\vec q} - \frac{1-x}{2}J_{\vec k-\vec q} - x\frac{\tilde t_{\vec q}^2}{E_{\rm ct}} - \frac{1+x}{2}\frac{2\tilde t_{\vec k}\tilde t_{\vec q}}{E_{\rm ct}}\right]K_{\vec q}\right.$$
$$\left. - \left[t_{\vec k-\vec q} - \frac{1-x}{2}\left(J_{\vec q} - \frac{\tilde t_{\vec k-\vec q}^2}{E_{\rm ct}}\right) - \frac{1+x}{2}\frac{2\tilde t_{\vec k}\tilde t_{\vec k-\vec q}}{E_{\rm ct}}\right]\frac{3}{2}C_{\vec q}\right\}. \tag{8}$$

Here N is the number of vectors in momentum space. Also, the static spin–spin correlation function

$$C_{\vec q} = \sum_{f,g} e^{-i(f-g)\vec q}\langle X_f^{\sigma\bar\sigma}X_g^{\bar\sigma\sigma}\rangle = 2\sum_{\vec r} e^{-i\vec r\vec q}\langle S_{\vec r}^z S_0^z\rangle, \tag{9}$$

and the kinematic correlation function

$$K_{\vec q} = \sum_{f,g} e^{-i(f-g)\vec q}\langle X_f^{\sigma 0}X_g^{0\sigma}\rangle, \tag{10}$$

were introduced.

Kinematic correlation functions (10) are calculated straightforwardly using the Green function (7). The spin–spin correlation functions for the t–J model with the three-site correlated hoppings H_3 were calculated in [29] and the following expression for the Fourier transform of the spin–spin Green function was derived:

$$\langle\langle X_{\vec q}^{\sigma\bar\sigma}|X_{\vec q}^{\bar\sigma\sigma}\rangle\rangle_\omega = \frac{A_{\vec q}(\omega)}{\omega^2 - \omega_{\vec q}^2}, \tag{11}$$

where $A_{\vec q}(\omega)$ and the magnetic excitations spectrum $\omega_{\vec q}$ are given in [29] by equations (25) and (26), respectively.

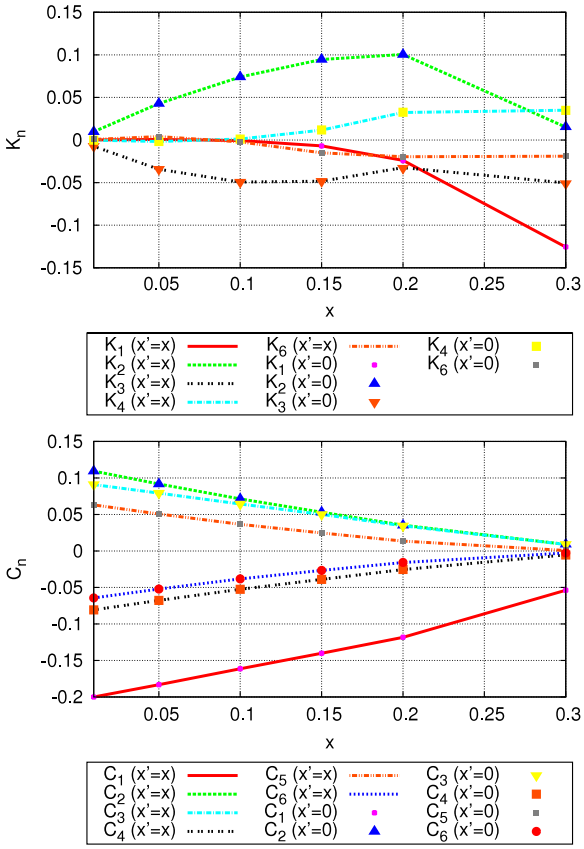

Figure 3. Doping-dependent evolution of the kinematic (upper panel) and the spin–spin (lower panel) correlation functions within the t–t'–t''–J^* model. Index n enumerates the real space vectors connecting the neighboring sites: $n = 1$ for the nearest-neighbors, $n = 2$ for the next nearest neighbors, and so on.

The following results were obtained by self-consistent calculation of the chemical potential μ, the spin–spin correlation functions (9) using the Green function (11), and the kinematic correlation functions (10) using the Green function (7) with the self-energy (8).

Parameters of the effective t–t'–t''–J^* model were obtained directly from the *ab initio* parameters of the multiband model, table 2. Their dependence on Ce concentration is presented in table 3. Note, here we took Cu-4s orbitals into account implicitly through the LDA + GTB method, as was described in section 3. However, within the Hubbard operators technique it is possible to take these orbitals into account explicitly using more cumbersome methods like the one introduced in [30].

Our results for the doping dependence of the kinematic and spin–spin correlation functions are shown in figure 3. Here, variable x' denotes the concentrations for which the one-electron parameters were calculated. Thus, $x' = 0$ corresponds to the absence of the one-electron mechanism of doping dependence, while $x' = x$ corresponds to the presence of this mechanism. However, the many-body mechanism is present in both cases. Note, the behavior of all correlation functions is almost identical for the cases of the presence and absence of the one-electron mechanism of doping dependence. Also note, the kinematic correlation functions, K_n, possess a very nontrivial doping dependence. For low concentrations, $x < 0.2$,

Table 3. Doping-dependence of the effective t–t'–t''–J^* model parameters (all values are in eV). Note, in the notations of [8] the hopping matrix elements t_{fg} correspond to $-t_{fg}^{00}$, and $\tilde{t}_{fg} = -t_{fg}^{0S}$. Also, $J_{fg} = 2\tilde{t}_{fg}^2/E_{\rm ct}$.

Parameter	$x = 0.00$	0.05	0.10	0.15	0.20	0.30
$-t \equiv -t_{01}$	0.552	0.560	0.561	0.572	0.572	0.567
$-t' \equiv -t_{11}$	−0.054	−0.053	−0.050	−0.056	−0.054	−0.052
$-t'' \equiv -t_{02}$	0.086	0.087	0.087	0.070	0.089	0.088
$J \equiv J_{01}$	0.463	0.477	0.484	0.488	0.492	0.486
$J' \equiv J_{11}$	0.007	0.007	0.007	0.007	0.007	0.007
$J'' \equiv J_{02}$	0.012	0.013	0.013	0.013	0.013	0.013
$-\tilde{t}_{01}$	0.680	0.691	0.695	0.699	0.701	0.697
$-\tilde{t}_{11}$	−0.085	−0.085	−0.081	−0.086	−0.084	−0.082
$-\tilde{t}_{02}$	0.111	0.112	0.112	0.113	0.113	0.112

due to the strong magnetic correlations the hoppings to the nearest neighbors are suppressed leading to the small value of K_1, while K_2 and K_3 are not suppressed. Upon increase of the doping concentration above $x \approx 0.2$, magnetic correlations decrease considerably and the nearest-neighbor kinematic correlation function K_1 increases, reviving the almost Fermi liquid behavior: K_1 becomes largest of all K_n values, while the magnetic correlation functions, C_n, are strongly suppressed.

So, we can clearly define one point of the crossover, namely, $x_m \approx 0.2$. The system behavior is quite different on the different sides of these point, although there is no phase transition when symmetry breaking occurs. Apparently, this crossover is closely connected to the change of the Fermi surface topology with doping. Fermi surface evolution together with the quasiparticle dispersion is shown in figure 4. For small x, the electron pockets around $(\pm\pi, 0)$ and $(0, \pm\pi)$ points are present at the Fermi surface. Upon increase of the doping concentration these pockets become larger and merge together at $x = 0.2$. For higher concentrations, the Fermi surface appears to be a large hole-like one, shrinking toward the (π, π) point. Thus, the topology of the Fermi surface changes at the same doping x_m, where the point of crossover is situated. For the first time the 'electronic transition' accompanying the change of the Fermi surface topology, or the so-called Lifshitz transition, was described in [31]. Now such transitions are referred to as quantum phase transitions with a co-dimension $= 1$ (see e.g. paper [32]).

Note, when the Fermi surface topology changes at a quantum critical concentration $x_m = 0.2$ the density of states at the Fermi level also exhibits significant transformation. This results in the different behavior of the kinematic and magnetic correlation functions on different sides of this crossover point, and, of course, the changes in the density of states at the Fermi level will also result in significant changes of such observable physical quantities as the resistivity and the specific heat.

Above the critical concentration, the Van Hove singularity in DOS is due to the flat dispersion around the $(\pi, 0)$ point. However, for $x < x_m$ this singularity is due to the states near the $(\pi/2, \pi/2)$ point. This is the result of many-body interactions that cannot be obtained within the one-electron band theory.

Concerning the role of the short range magnetic order and three-site hopping terms in the n-type cuprates, we would like to stress that due to the scattering on the magnetic excitations with the AFM wavevector $\vec{Q} = (\pi, \pi)$ the states near the (π, π) point are pushed above the Fermi level, and the local symmetry around the $(\pi/2, \pi/2)$ points is restored for low doping concentrations (see figure 4). In other words, the short range magnetic order 'tries' to restore

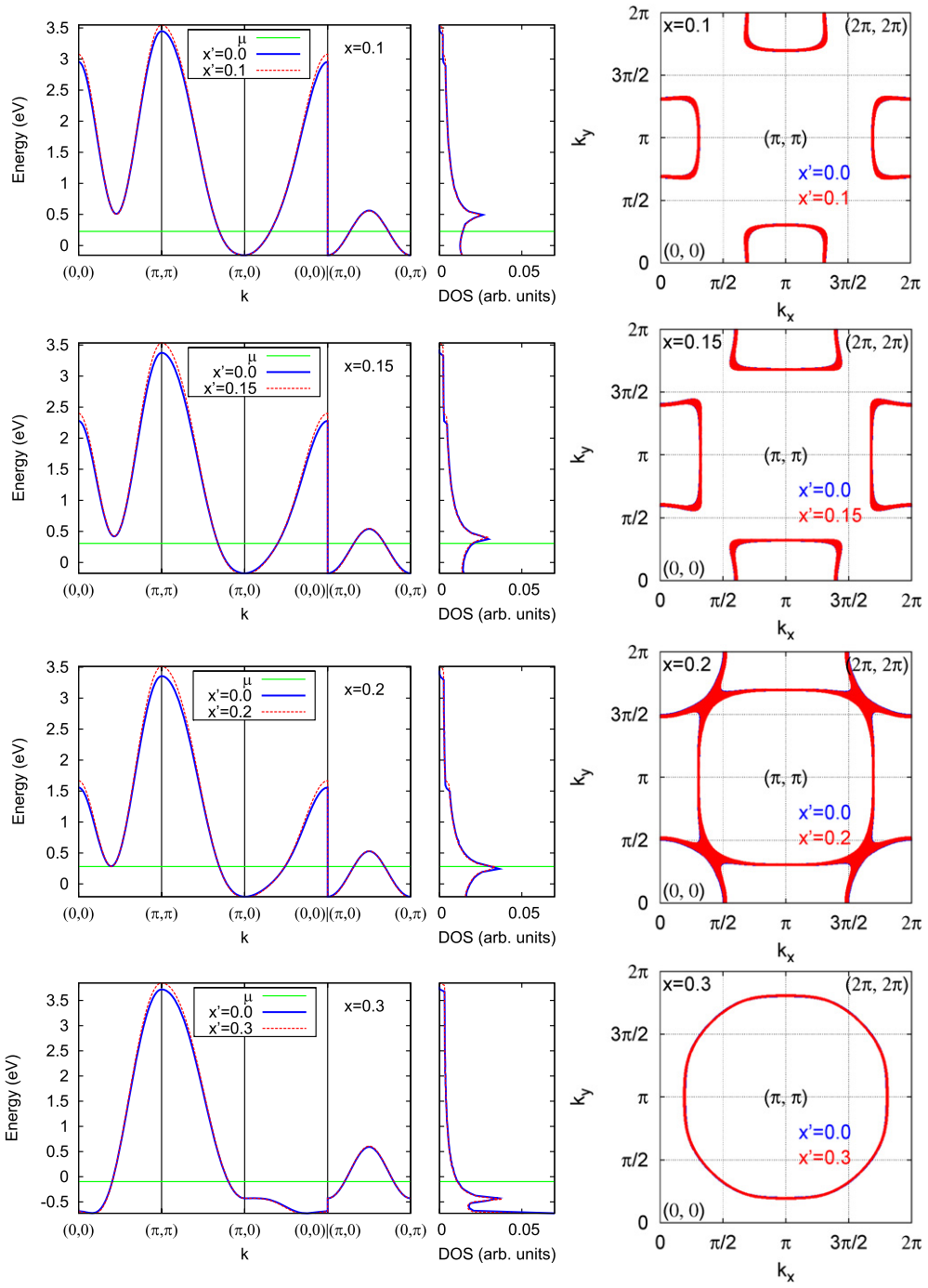

Figure 4. Doping-dependent quasiparticle dispersion (on the left) and Fermi surface (on the right) in the spin-liquid phase of n-type cuprates. The position of the chemical potential is denoted by the horizontal (green) line. The solid (blue) curves correspond to the calculations without taking the one-electron mechanism of concentration dependence into account ($x' = 0$ case). The dashed (red) curves represent results of the calculations in which both many-body and one-electron mechanisms were considered ($x' = x$ case). Note, the Fermi surfaces for both $x' = 0$ and $x = x$ cases are almost indistinguishable.

the AFM symmetry around the $(\pi/2, \pi/2)$ point. In our calculations, the short range magnetic fluctuations are taken into account via the spin–spin correlation functions (9).

Now we proceed to the comparison of the one-electron and many-body mechanisms of the doping dependence. In figure 4 the quasiparticle dispersion without the one-electron mechanism is shown by the solid (blue) curves. Apparently, its difference from the case when both one-electron and many-body mechanisms are present is negligibly small. In the latter case the bandwidth is slightly renormalized while band dispersion retains the same character. Moreover, the Fermi surfaces for both cases are very similar and the quantum phase transition will be at the same concentration, $x_m = 0.2$.

6. Conclusion

In the present work we report the combined investigation of the one-electron and the many-body mechanisms of the electronic structure doping dependence for the high-T_c compound $Nd_{2-x}Ce_xCuO_4$. The electronic structure calculations were performed within the hybrid LDA + GTB scheme. For both the antiferromagnetic and paramagnetic spin-liquid phases we demonstrate that the main effect on the electronic structure is provided by the many-body mechanism, whereas the one-electron contribution leads to small quantitative modifications which do not change the picture qualitatively. The role of the many-body mechanism is very important because of the strong electronic correlations present in the underdoped cuprates.

Acknowledgments

This work was supported in part by RFBR Grants 06-02-16100 (MMK, VAG, SGO), 06-02-90537-BNTS (MMK, VAG, SGO, IAN, ZVP), 05-02-16301 (IAN), 05-02-17244 (IAN), by the joint UrO-SO project 74, and programs of the Presidium of the Russian Academy of Sciences (RAS) 'Quantum macrophysics' and of the Division of Physical Sciences of RAS 'Strongly correlated electrons in semiconductors, metals, superconductors and magnetic materials'. MMK acknowledge support form INTAS (YS Grant 05-109-4891). IAN and ZVP acknowledge support from the Dynasty Foundation and International Center for Fundamental Physics in the Moscow program for young scientists. IAN appreciates the support from the grant of the President of the Russian Federation for young PhD MK-2242.2007.02. ZVV is supported by a UrO grant for young scientists.

References

[1] Massidda S, Hamada N, Yu J and Freeman A J 1989 *Physica* C **157** 571
[2] Yu J and Freeman A J 1991 *Physica* C **173** 274
[3] Yu J and Freeman A J 1991 *J. Phys. Chem. Solids* **52** 1351
[4] Mishonov T and Penev E 2000 *J. Phys.: Condens. Matter* **12** 143
[5] Andersen O K, Liechtenstein A I, Jepsen O and Paulsen F 1995 *J. Phys. Chem. Solids* **56** 1573
[6] Andersen O K, Savrasov S Y, Jepsen O and Liechtenstein A I 1996 *J. Low Temp. Phys.* **105** 285
[7] Pavarini E, Dasgupta I, Saha-Dasgupta T, Jepsen O and Andersen O K 2001 *Phys. Rev. Lett.* **87** 047003
[8] Korshunov M M, Gavrichkov V A, Ovchinnikov S G, Nekrasov I A, Pchelkina Z V and Anisimov V I 2005 *Phys. Rev.* B **72** 165104
[9] Gavrichkov V A, Ovchinnikov S G, Borisov A A and Goryachev E G 2000 *Zh. Eksp. Teor. Fiz.* **118** 422
Gavrichkov V A, Ovchinnikov S G, Borisov A A and Goryachev E G 2000 *JETP* **91** 369 (Engl. Transl.)
[10] Gavrichkov V A and Ovchinnikov S G 2004 *Zh. Eksp. Teor. Fiz.* **125** 630
Gavrichkov V A and Ovchinnikov S G 2004 *JETP* **98** 556 (Engl. Transl.)
[11] Kamiyama T, Izumi F, Takahashi H, Jorgensen J D, Dabrowski B, Hitterman R L, Hinks D G, Shaked H, Mason T O and Seabaugh M 1994 *Physica* C **229** 377

[12] Paulus E F, Yehia I, Fuess H, Rodriguez J, Vogt T, Ströbel J, Klauda M and Saemann-Ischenko G 1990 *Solid State Commun.* **73** 791
[13] Andersen O K and Jepsen O 1984 *Phys. Rev. Lett.* **53** 2571
[14] Andersen O K, Pawlowska Z and Jepsen O 1986 *Phys. Rev.* B **34** 5253
[15] Singh D J 1991 *Phys. Rev.* B **44** 7451
[16] Emery V J 1987 *Phys. Rev. Lett.* **58** 2794
[17] Varma C M, Smitt-Rink D and Abrahams E 1987 *Solid State Commun.* **62** 681
[18] Andersen O K and Saha-Dasgupta T 2000 *Phys. Rev.* B **62** 16219(R)
[19] Anisimov V I, Korotin M A, Nekrasov I A, Pchelkina Z V and Sorella S 2002 *Phys. Rev.* B **66** 100502
[20] Gunnarsson O, Andersen O K, Jepsen O and Zaanen J 1989 *Phys. Rev.* B **39** 1708
[21] Hubbard J C 1963 *Proc. R. Soc.* A **276** 238
[22] Zaitsev R O 1975 *Sov. Phys.—JETP* **41** 100
[23] Izumov Yu and Letfullov B M 1991 *J. Phys.: Condens. Matter* **3** 5373
[24] Ovchinnikov S G and Val'kov V V 2004 *Hubbard Operators in the Theory of Strongly Correlated Electrons* (London: Imperial College Press)
[25] Hubbard J C 1964 *Proc. R. Soc.* A **277** 237
[26] Ovchinnikov S G, Borisov A A, Gavrichkov V A and Korshunov M M 2004 *J. Phys.: Condens. Matter* **16** L93
[27] Korshunov M M and Ovchinnikov S G 2006 *Eur. Phys. J.* B **57** 271
[28] Plakida N M, Yushankhai V Yu and Stasyuk I V 1989 *Physica* C **162–164** 787
[29] Val'kov V V and Dzebisashvili D M 2005 *Zh. Eksp. Teor. Fiz.* **127** 686
Val'kov V V and Dzebisashvili D M 2005 *JETP* **100** 608 (Engl. Transl.)
[30] Digor D F, Entel P, Moskalenko V A and Plakida N M 2006 *Theor. Math. Phys.* **149** 1382
[31] Lifshitz I M 1960 *Sov. Phys.—JETP* **11** 1130
[32] Volovik G E 2006 *Acta Phys. Slovaca* **56** 49
Volovik G E 2006 *Preprint* cond-mat/0601372